AGU PUBLICATIONS

JGR

Journal of Geophysical Research: Atmospheres

RESEARCH ARTICLE
10.1002/2014JD021949

Key Points:
- The radiative effects due to ash deposition onto Arctic snow are quantified
- Ash deposits can have greater radiative impacts than dust or black carbon
- Ash from midsized eruptions can be a major agent of deposit-induced snowmelt

Supporting Information:
- Readme
- Supporting figures

Correspondence to:
C. L. Young,
cindy.young@eas.gatech.edu

Citation:
Young, C. L., I. N. Sokolik, M. G. Flanner, and J. Dufek (2014), Surface radiative impacts of ash deposits from the 2009 eruption of Redoubt volcano, *J. Geophys. Res. Atmos.*, *119*, 11,387–11,397, doi:10.1002/2014JD021949.

Received 6 MAY 2014
Accepted 15 SEP 2014
Accepted article online 18 SEP 2014
Published online 10 OCT 2014

Surface radiative impacts of ash deposits from the 2009 eruption of Redoubt volcano

Cindy L. Young[1], Irina N. Sokolik[1], Mark G. Flanner[2], and Josef Dufek[1]

[1]School of Earth and Atmospheric Sciences, Georgia Institute of Technology, Atlanta, Georgia, USA, [2]Department of Atmospheric, Oceanic and Space Sciences, University of Michigan, Ann Arbor, Michigan, USA

Abstract The solar broadband albedo change, surface radiative forcing, and snowmelt rate associated with ash deposits based on those from the 2009 eruption of Redoubt volcano were calculated using the field-corroborated loadings from the Fall3D and the SNow, ICe, and Aerosol Radiation models. The optical properties of ash were calculated from Mie theory, using size information from the Fall3D model. Two sizes of snow grains were used in order to simulate a young and old snowpack. The results show concentrations of aerosol-sized ash in snow range from ~6.9×10^4 to 1×10^8 ppb, for the distal edge of the deposits (located ~100–570 km from the vent) to the vent, and integrated solar albedo reductions of ~0–59% for new snow and ~0–85% for old snow. These albedo reductions are much larger than those typical for black carbon and are of the same order of magnitude as those reported for volcanic deposits in Antarctica. The daily mean surface shortwave forcings associated with ash deposits on snow were ~0–96 W m^{-2} from the most distal deposits to the near-vent deposits. We show that forcings caused by ash deposits can be greater than those caused by dust deposits. There were no accelerated snowmelts calculated for the edges of the deposits. However, for areas of higher ash concentrations, daily melting rates were conservatively estimated to be ~140–160% higher than those of pure snow. We find that ash deposits from midsized volcanic eruptions can be a major agent of deposit-induced snowmelt.

1. Introduction

The climate of the Arctic region is especially sensitive to perturbations in the regional radiative energy budget [e.g., *Curry et al.*, 1996; *Langen and Alexeev*, 2007]. An important modulator of Arctic radiation climate is the presence of aerosols [*Shindell*, 2007], both natural and anthropogenic. The radiative effects of smoke, dust, and haze in the Arctic have been well studied [e.g., *Stone et al.*, 2007, 2008; *Quinn et al.*, 2008], but the impacts of volcanic aerosols on the Arctic environment have received less attention [*Young et al.*, 2012; *Flanner et al.*, 2014]. Compared to the more predictable seasonal frequencies of the occurrences of smoke, dust, and haze, volcanic eruptions in the Arctic region occur unexpectedly and quite frequently. Here we use the term "Arctic region" to include both the true Arctic that lies within the Arctic Circle (north of 66.5 N) and the sub-Arctic (50–66.5 N). This definition was chosen because both the true Arctic and sub-Arctic are more sensitive to radiative perturbations than lower latitudes, and volcanoes in either region can transport and deposit ash into the other. As of April 2014, there are ~ three volcanoes experiencing activity north of 54°N (http://www.volcano.si.edu/). Although the durations and intensities of eruptions can vary, volcanic eruptions have the capacity to be long duration (months to years) [*Simkin and Siebert*, 1994] and high intensity events, expelling large amounts of ash and gases into the atmosphere. Volcanic ash is defined as tephra having a diameter < 2 mm, and ash does include an aerosol-sized fraction (diameter ≤ 100 μm).

Young et al. [2012] calculated a range of radiative effects that can be expected for a plume from a typical midsized Arctic eruption and compared the magnitudes of the effects to those for plumes of the other aerosol types typical to the Arctic environment. It was found that volcanic plumes with compositions rich in ash can have magnitudes of forcing which are much larger than those for other aerosol types under the same environmental conditions [*Young et al.*, 2012]. Volcanic deposits are expected to have even larger radiative impacts than plumes because surface deposits can remain long after a volcanic plume has passed over and dissipated. In addition, the region lying within the Arctic Circle is the second largest desert in the world. As such, little snowfall would cover ash deposits, although winds could scatter them, reducing their surface loadings. Ash deposits in the wetter sub-Arctic region are more likely to be covered by snow layers, reducing the radiative impacts. However, one composite ash layer would form on top of the snowpack once the snow

Table 1. Dates and Times (UTC) for Major Land-Depositing Events From the 2009 Eruption of Redoubt Volcano

Event Number	Date (UTC)	Time (UTC)
2	3/23/2009	7:02
3	3/23/2009	8:14
4	3/23/2009	9:38
5	3/23/2009	12:30
6	3/24/2009	3:40

began to melt, either accelerating or decelerating further snowmelt, depending on the thickness of this layer. Deposition of solar absorbing particles, such as soot, dust, and volcanic ash, has been shown to alter surface albedo and cause early snowmelts, which can have profound impacts on the regional climate and hydrologic cycle [*Qian et al*., 2009]. The radiative impacts of dust [*Painter et al*., 2010] and soot [*Flanner et al*., 2007] deposits onto ice and snow surfaces have been studied. There have been few considerations of the radiative impacts of volcanic ash deposits in snow [e.g., *Driedger*, 1981; *Warren*, 1984; *Dadic et al*., 2013]. Despite the potential of volcanic ash deposits to significantly alter surface reflectivity, there are even fewer studies that assess the surface radiative impacts of volcanic ash deposits from an Arctic eruption or comprehensively cover the entire deposit region [e.g., *Flanner et al*., 2014].

The 2009 eruption of Redoubt volcano in Alaska, USA (60.49 N, 152.74 W) was selected as a case study because it produced extensive ash deposits that stretched hundreds of kilometers in all directions from the volcanic source [*Schaefer*, 2012; *Young et al*., 2014] and was associated with early snowmelt [*Schaefer*, 2012]. According to the Alaska Volcano Observatory (AVO), Alaska experiences on average two volcanic eruptions per year. The 2009 eruption of Redoubt Volcano was considered a midsized volcanic eruption, based on the volcanic explosivity index (VEI) [*Wallace et al*., 2013]. Small to midsized volcanic eruptions occur more frequently than larger eruptions in the Aleutian arc and provide an intermittent source of ash and gases to the environment.

The goal of this work is not to determine an exact radiative impact of ash deposits associated with the Redoubt eruption, but to assess a range of realistic surface albedo change and radiative forcing due to ash deposition that can be expected from a typical midsized volcanic eruption, using the ash loading fields reported for the 2009 eruption of Redoubt volcano in *Young et al*. [2014], which were corroborated by satellite and field data. We assess the possible hydrological importance of this type of eruption by making estimates of snowmelt amounts, and we compare the calculated surface albedo change and radiative forcing to other depositional events associated with different aerosol types (i.e., black carbon and dust).

2. Methodology

2.1. The SNICAR Model

The SNow, ICe, and Aerosol Radiation (SNICAR) model [e.g., *Flanner and Zender*, 2005, 2006; *Flanner et al*., 2007] was employed to calculate the solar albedo change and net radiative flux fields at the surface produced by total cumulative ash deposits from the major land-depositing events from the March 2009 eruption of Redoubt volcano in Alaska, USA (Table 1). The SNICAR model allows the user to choose from different two-stream approximations of the radiative transfer equation, and a multilayer solution from *Toon et al*. [1989], to solve the plane parallel radiative transfer equation for multiple layers in snow. In allowing for multiple layers, the model can address the vertical differences in snow and impurity properties. This work utilizes a hemispheric mean two-stream approximation [*Toon et al*., 1989], because other approximations can give unphysical results in the near-infrared. Therefore, the hemispheric mean was deemed more appropriate for a larger variety of situations, including calculating shortwave broadband albedos and surface fluxes. The model requires solar zenith angle (SZA) and underlying surface spectral or monochromatic reflectance, snow layer properties (i.e., snow layer thickness, snow density for each layer, and snow effective radius), and impurity properties (i.e., particle mass mixing ratios, effective radius, and refractive index).

A spectrally constant underlying surface reflectance between 0.17 and 0.3 was used to simulate snow cover on surfaces ranging from volcanic rock [*Tsvetsinskaya et al*., 2002] to glacier ice [*Knap et al*., 1999], respectively, although the model is not sensitive to this parameter with the large snow depths used in this study. At approximately 60°N, the highest SZA for a day in mid-March is 55°. A lower SZA of 75° was chosen to represent a middle point between the highest and lowest daily Sun angles. Spectral solar flux distributions from the sub-Arctic summer atmospheric profile used by *McConnell et al*. [2007] to represent clear-sky

conditions in Greenland, along with the total incident surface flux calculated from the Santa Barbara Disort Atmospheric Radiative Transfer model, were used to compute spectral direct-beam incident fluxes. Daily snow layer thickness from the Natural Resources Conservation Service's SNow TELemetry (SNOTEL) for Alaska sampling stations was used to estimate snow layer thickness and snow water equivalent (SWE). Snow density was computed from SWE data. A snow layer that was representative of measurements from the Alaska stations was selected, which had a total snow depth of 1 m and a snow density of 190 kg m^{-3}. Effective snow grain size radius can range from 50 to 1100 μm [e.g., *Painter et al*., 2003], with older snow having larger grains. Profiles of snow effective radius for the region and times of the eruption were not available. Therefore, a snow grain radius of 100 μm was selected to represent newer snow, and a radius of 1000 μm was selected to simulate aged snow. Optical properties of ice from *Warren et al*. [2006] were used.

2.2. Determining Particle Mixing Ratios and Ash Grain Sizes

Particle mixing ratio fields of ash in snow (in ppb by mass) were determined from total cumulative ash deposit loading fields taken from *Young et al*. [2014] for the entire period of major land-depositing events (23 and 24 March), listed in Table 1. In *Young et al*. [2014], input parameters for the Fall3D volcanic ash dispersion and transport model (VADTM) [*Folch et al*., 2009; *Costa et al*., 2006] were systematically varied over a realistic range of values for eruptions of this type obtained from field measurements and the literature. Those parameters which produced the best agreement with satellite and field data were employed in the best fit simulation on which all loadings and grain sizes used in this study are based. The modeled ash plumes and deposits reported in *Young et al*. [2014] showed good to moderate agreement with satellite data and field measurements presented by *Wallace et al*. [2013]. Modeled depositional loading fields were used here instead of measured loading fields because we were interested in studying the radiative impacts of aerosol-sized ash across the entire deposit. The depositional maps from *Wallace et al*. [2013] did not cover the entire area of the aerosol-sized deposits, and the measured area only covers those deposits in closer vicinity to the vent, where less aerosol-sized ash fell. Although these deposits were very well-sampled for such a rugged environment, these are still not resolved enough to achieve our goals. Modeled depositional loading fields were translated into mixing ratios using the density of snow (190 kg m^{-3}) and assuming all ash is in the top centimeter of the snowpack. This was selected as a reasonable depth because the total measured and modeled thickness of ash deposits did not exceed 1 cm in the more distal areas of ashfall, and little mixing into deeper layers was expected. The assumption of spherical ash particles (sphericity = 1) in the transport model produces better agreement with field measurements of deposit loadings, except in locations that are ≥210 km from the volcanic vent. In these regions, nonspherical particles (sphericity = 0.7) produce loadings that agree better with field data. Therefore, we used loading fields produced by spherical particles for locations < 210 km and loading fields of nonspherical particles (sphericity = 0.7) for locations ≥210 km. The effects of loading variations on modeled integrated solar albedo are discussed. The Fall3D was used in a setup similar to that of *Young et al*. [2014] to produce spatial fields of deposited ash median radius and standard deviation, and a measured initial grain size distribution from *Mastin et al*. [2013] was used. For the model, a total mass of 5×10^{10} kg of ash was erupted into the atmosphere. The mass erupted for each event was determined by multiplying the mass flow rate [*Mastin et al*., 2013; *Young et al*., 2014] by the event duration [*Wallace et al*., 2013], and the total mass was calculated by summing the individual erupted masses for each event.

2.3. Ash Microphysical Model

The optical properties of the ash were computed according to Mie theory for a lognormal particle distribution, using total cumulative deposited ash mean effective radii and standard deviation fields calculated from Fall3D and the spectral refractive indices for andesitic ash [*Pollack et al*., 1973]. The shortwave imaginary components of the refractive index for ash [*Pollack et al*., 1973] are similar to those reported for dust [*Smith and Grainger*, 2014], but the refractive index of black carbon is 2 orders of magnitude larger [*Wang et al*., 2013]. Although consideration of nonspherical particles is an important part of determining total cumulative ash deposit loadings [*Young et al*., 2014], only spherical particles were considered in calculating the optical properties of ash. This is because the single scattering properties of nonspherical particles in radiative flux calculations are well approximated using equal volume to projected area ratio spheres [*Fu et al*., 2009; *Flanner et al*., 2014]. Only aerosol-sized ash particles (radius ≤50 μm) were considered in this study. This is because the larger sized ash particles are minor in abundance and confined to areas very close to the vent [*Wallace et al*., 2013]. Therefore, the albedo reductions presented here for proximal deposits represent a lower bound.

Table 2. Stratigraphy of Sample Used to Investigate Sensitivity of Albedo to Snow Layers on Top and Between Ash Layers[a]

Thickness (cm)	Layer Description	Ash Concentration (ppb)	Solar Albedo of Composite Layer
43.0	snow	0	0.8448
0.5	ash	1×10^8	0.3581
0.5	snow	0	0.6810
0.5	ash	1×10^8	0.3584
55.5	snow	0	0.7316

[a]The sample was taken at 60.67 N, 152.77 W (~9 km from Double Glacier). The base snow layer is assumed to be old snow (radius = 1000 μm), and subsequent layers are treated as new snow (radius = 100 μm), as it would have been on 31 March 2009 when the layer was measured. A base layer of 55.5 cm is included, based on total snow depths from SNOTEL. Solar broadband albedos reported for every layer above the base snow layer include the layers beneath them.

2.4. The Snow/Ash Layering Structure

In the SNICAR model, cumulative ash deposits were deposited on top of the snowpack. Although initially ash deposits might be blanketed by new snow, this new snow will have a reduced longer-term effect on albedo. This is because ash is a hydrophobic particle and will not be incorporated into deeper layers of the snowpack as the snow melts. Rather, ash will be concentrated at the surface as the melt water trickles through the snow matrix, straining the ash out at the top layer of the snowpack [*Conway et al.*, 1996]. All of the ash for cumulative deposits is assumed to be concentrated in the top centimeter of the snowpack.

Some regions did experience new snowfall on top of the ash layer [*Schaefer and Wallace*, 2012]. It should be noted that the blanketing of new snow over ash deposits, especially over older snow, can significantly increase the albedo of the surface, depending on the thickness of the new snow layer and the concentration of the underlying deposit, which may lead to a positive bias in modeled radiative forcing. The locations and stratigraphic descriptions of a few sampling locations were provided by Janet Schaefer and Kristi Wallace of AVO. Snowfall during the eruptive events was highly variable even between nearby locations, making mapping of snowfall and ash/snow stratigraphy across the entire deposit region unfeasible. Additionally, no detailed time series data are available for how the layers evolve as the snow melts. Therefore, a representative layering structure was chosen from one sample site (60.67 N, 152.77 W) proximal to the vent to study the sensitivity of albedo to snowfall layered on top of and in between ash layers (Table 2). The base snow layer is assumed to be old snow (radius = 1000 μm), and subsequent layers are treated as new snow (radius = 100 μm), as it would have been on 31 March 2009 when the layer was measured. A base layer of 55.5 cm is included, based on total snow depths from SNOTEL. It should also be noted that winds could blow and disperse ash initially, but after some melting has occurred, the particles become wetted and adhere to the snow [*Schaefer*, 2012]. Therefore, the dispersion of deposits by wind is not considered here in assessing a range of radiative impacts from a typical midsized Arctic eruption.

2.5. Estimating Snowmelt Rates

Snowmelt estimations were made using the restricted degree-day radiation balance approach described in *Melloh* [1999]:

$$M = r\ T_d + m_Q F_{\text{net, SW}} \tag{1}$$

where M is the snowmelt (cm d^{-1}), r the constant-restricted degree-day factor (cm d^{-1} °C^{-1}), T_d the daily mean temperature over 24 h (°C), m_Q a physical constant converting radiation to SWE and is equal to 0.026 cm d^{-1} (W m^{-2})$^{-1}$, and $F_{\text{net SW}}$ the net solar surface radiation (W m^{-2}) calculated by the SNICAR model. *Martinec* [1989] showed that the values of r vary only slightly, from 0.20 to 0.25 cm d^{-1} °C^{-1}, throughout the snowmelt period. According to *Kustas et al.* [1994], low values of r occur when low relative humidity increases latent heat loss due to evaporation. Because the Arctic air is very dry, an r value of 0.20 cm d^{-1} °C^{-1} is appropriate.

3. Results and Discussion

The median ash radius across a lognormal mass size distribution of all ash deposit sizes decreases with distance from the volcanic vent (Figure 1a) and is comparable to the mass median radii of deposits measured

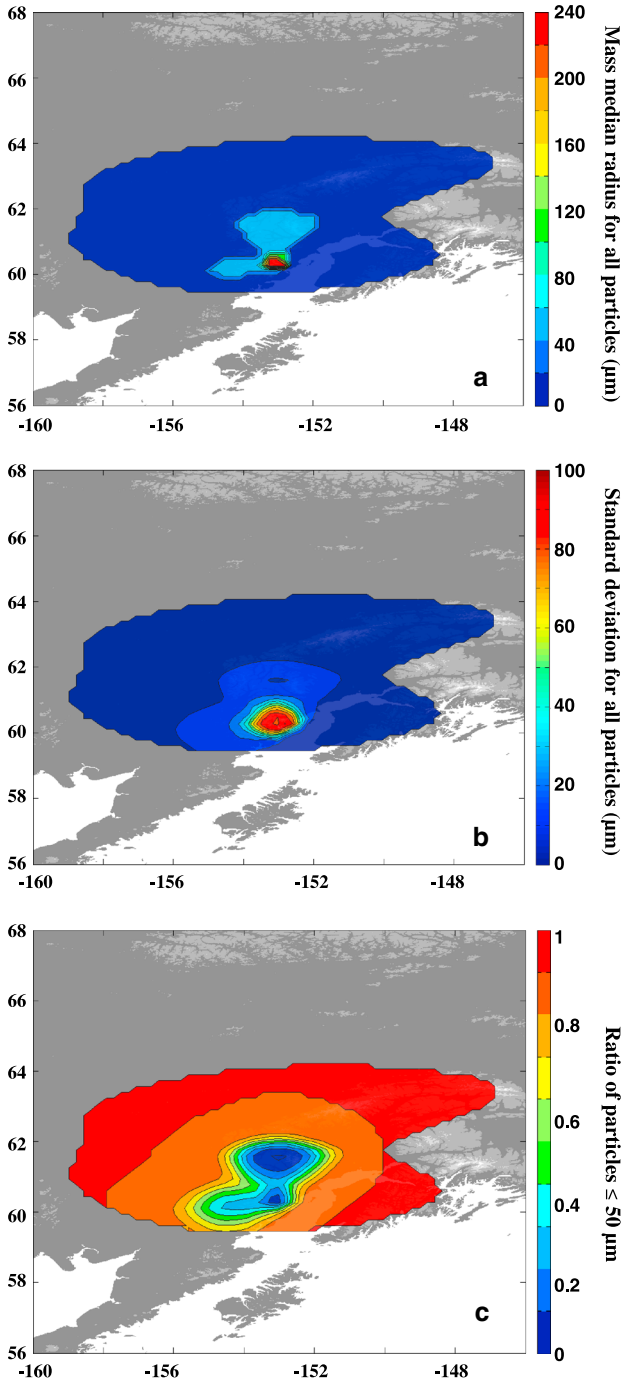

Figure 1. (a) Mass median radius for all particle sizes, (b) standard deviation for all particle sizes (μm), and (c) fraction of ash deposits that are aerosols (≤50 μm). The last contour in all plots corresponds to a loading of 0.1 g m^{-2}, as in *Young et al.* [2014].

by *Mastin et al.* [2013] for this eruption at 4 points located at various distances from the vent (Table 3). The median radii from *Mastin et al.* [2013] are similar to those modeled at the same distances, except for at the closest distance to the vent (12 km), where the measured radius is an order of magnitude larger than the modeled radius. As discussed by *Mastin et al.* [2013], this discrepancy is most likely due to the effect of particle aggregation occurring near the vent (see *Wallace et al.* [2013] for a complete description of particle aggregation during the eruption), which is not accounted for in the Fall3D model or any other VADTM to date. The standard deviation of the deposit size distribution decreases with increasing distance from the vent (Figure 1b). As larger sizes are removed and the number of size bins decrease, the spread of the distribution also decreases moving toward the edges of the deposits. The fractions of ash that are in the aerosol size range are shown in Figure 1c. The aerosol size fraction is carried further than larger sizes; and therefore, the ratio of aerosol ash to total ash increases with distance from the vent. The median radii for only ash sizes ≤ 50 μm is 15.75 μm on the northern boundaries of the deposits (above ~62.5 N) and 31.25 μm in all other deposits, across the domain shown in Figure 1. The median radius does not vary much spatially because of comparatively few size bins reported for aerosol-sized deposits [*Mastin et al.*, 2013], and the spread for the distributions is small. This is a direct result of the use of discrete size bins, and in nature, more spread is expected.

In order to calculate a range of reasonable albedo changes caused by ash deposits, the albedos of pure snow for the selected snow grain size radius and SZA must first be calculated using SNICAR. At a SZA of 75°, the solar integrated albedo is 0.8476 and 0.7394, for grain sizes of 100 μm and 1000 μm, respectively. Coarser-grained, older snow is optically darker, because the radiation must travel through a greater path of ice to get the same amount of extinction, increasing the probability of a photon being absorbed [*Flanner et al.*, 2007].

The albedos computed for ash deposits are subtracted from albedos of pure snow to obtain the change in albedo caused by the deposits. Reductions in integrated solar albedo, calculated by weighting with the surface-incident spectral fluxes, for a snow grain size of 100 μm are shown in Figure 2a and range from 0.4969

Table 3. Measured and Modeled Mass Median Radius for All Particle Sizes at Four Distances North of the Volcanic Vent

	Mass Median Radius (μm)	Mass Median Radius (μm)
Distance (km)	*Mastin et al.* [2013]	Modeled With Fall3D
218	≤ 31	15.75–31.25
120	≤ 31	31.25
29	125	62.5
12	1000	250

closest to the vent to 0.0023 on the edges of the deposits, around a loading of 0.1 g m^{-2} in the snowpack. The high and low albedo change values corresponded to concentrations of ~1×10^8 and 6.9×10^4 ppb, respectively. Because the median radius over which optical calculations were performed did not vary much across the deposits, the optical properties of the aerosol-sized ash deposits were similar across much of the region. Therefore, much of the variation in the albedo reduction fields is due to the ash loading, making loading assessments the most important part of these analyses. Solar integrated albedo reductions for snow grain size of 1000 μm are displayed in Figure 2b. These values vary from 0.6293 closest to the vent to 0.0029 on the edges of the deposits. The large snow grain size and the increasing amounts of ash moving closer to the vent amplify the reduction in albedo. This causes the larger changes in albedo that occur further from the vent in Figure 2b when compared to Figure 2a.

The sensitivity of solar albedo to snow layers in between and on top of ash layers was investigated using stratigraphy base on a personal communication from Janet Schaefer and Kristi Wallace (2014) for a sampling site located in close proximity to the volcanic vent (Table 2). The ash layer thicknesses reported in the field include any incorporated snow, and snow layer thicknesses are for pure snow. There was an ash layer reported below the first ash layer, but this layer contained tephra larger than the sizes considered in this study and was not included. Modeling this layer as aerosol had no effect on the resulting albedo of the bottom ash layer. Integrated solar albedos were calculated for the bottom snow layer of 55.5 cm and each layer above it. Albedos reported for every layer above the bottom snow layer include the layers beneath them. We observe that the effect of snow between and on top of ash deposits is to increase the albedo substantially. Even a snow layer of 0.5 cm over a highly concentrated ash layer can increase albedo from ~0.36 to ~0.68. However, a similarly highly concentrated layer of ash deposited on top of the 0.5 cm of snow can be just as absorbing as the first ash layer. The largest factor impacting albedo is the 43 cm of new snow on top of all ash and snow layers. This new snow causes the composite layer to be even more reflective than it was before the ash was deposited because it is more reflective than the old snow underneath. This top layer of snow causes there to be initially no reduction of albedo due to ash

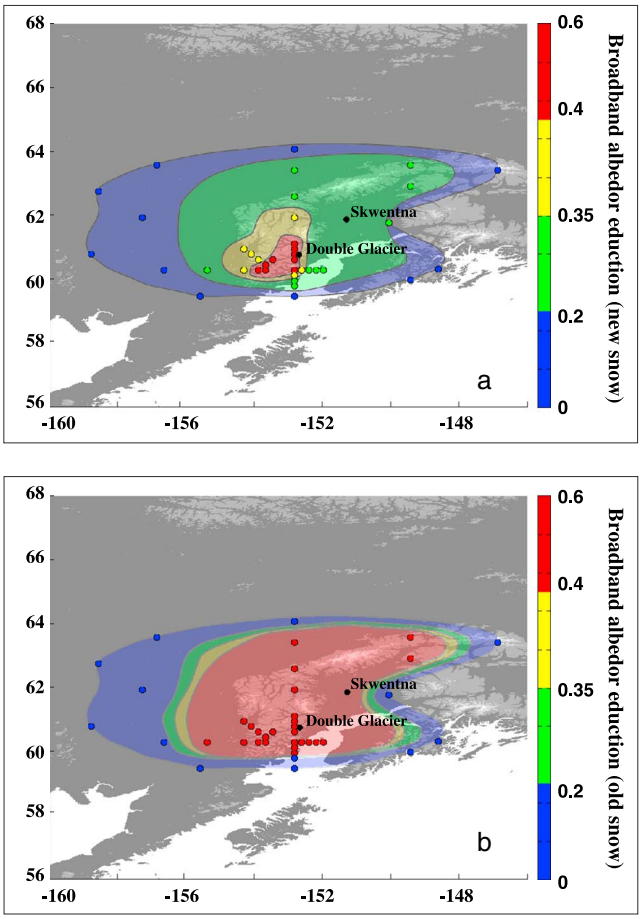

Figure 2. Range of realistic reductions in solar broadband albedo for (a) ash deposits on new snow (effective radius = 100 μm) and (b) ash deposits on old snow (effective radius = 1000 μm). Note that Fall3D and SNICAR are not coupled, so fields were drawn based on calculations made at several points, which are denoted by circles.

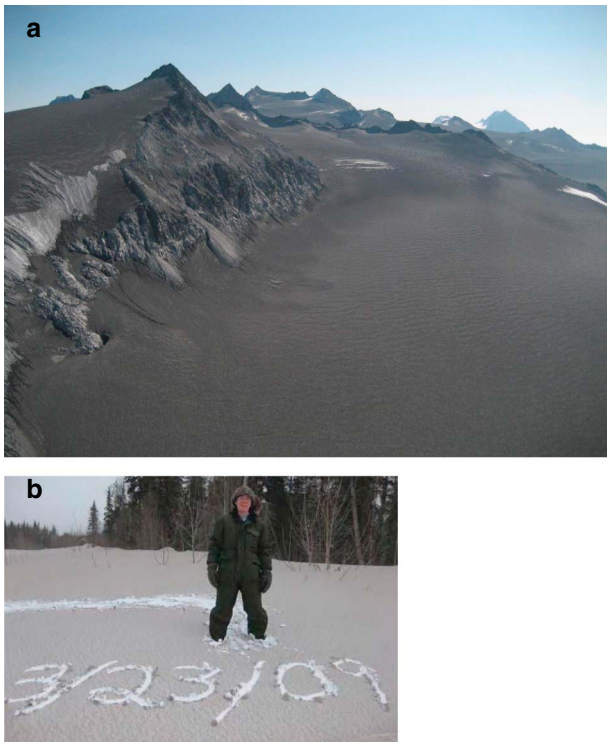

Figure 3. (a) Complete ash coverage at Double Glacier (60.72 N, 152.67 W) on 10 June 2009. This photo was taken by Max Kaufman at Alaska Volcano Observatory/University of Alaska Fairbanks, Geophysical Institute. (b) Complete ash coverage near Skwentna (61.90 N, 151.25 W). Photo courtesy of the Department of Natural Resources [*Schaefer*, 2012].

deposition. However, in sunlit regions where temperatures are high enough to melt the snow, this initial state may change rapidly.

We were unable to obtain satellite observations of albedo for deposits from this eruption, because bright surfaces and clouds were a constant issue for retrievals. We are also unaware of any relevant field measurements of albedo. Albedo is typically not measured by scientists at volcano observatories, who are often first on the scene after an eruptive event. For scientists interested in the immediate radiative impacts of ash deposits, field travel is near impossible to plan due to the unpredictability and the dangers of volcanic eruptions. Time series investigations of how the ash and snow layers evolve through time are even more challenging to perform. Citizen scientists did document and photograph the extent of ash deposit coverage in their areas, and these reports are published by *Schaefer* [2012]. Citizens observed complete coverage of the surface by ash at Bentalit Lodge, near Skwentna (61.90 N, 151.25 W) [*Schaefer*, 2012], and complete ash coverage was also photographed by AVO ~9 km from the sampling site reported in Table 2 at Double Glacier (60.72 N, 152.67 W) (Figure 3). Based on these accounts, it is expected that the albedo reduction would be significant for these regions. Significant albedo reductions are observed in Figures 2a and 2b near Skwentna and Double Glacier. The ash at Double Glacier became one composite ash layer as the snow layers melted and remained until at least June 2009 to be photographed. This further illustrates that modeling ash as one composite layer can capture much of the longer-term radiative impacts, even in a sub-Arctic environment that experiences snowfall over ash deposits. This would especially be true for permanently glaciated regions that receive ample sunlight for melt to occur and/or little precipitation to cover the ash deposits, as in the true Arctic.

Here we estimate concentrations of ash in snow that range from ~6.9×10^4 to 1×10^8 ppb, and possible integrated solar albedo reductions of ~0–59% for new snow and ~0–85% for old snow. Some typical concentrations of black carbon in snow are ~5–50 ppb corresponding to a spectrally averaged albedo reduction of ~1–3% [*Clarke and Noone*, 1985; *Warren and Wiscombe*, 1985]. Although black carbon would be expected to be more absorbing than volcanic ash for a similar particle size and concentration, the extreme loadings that can be present from a midsized volcanic eruption produce albedo changes that dwarf those due to black carbon. Integrated solar albedos for volcanic deposits in Antarctica were reported by *Dadic et al*. [2013]. It was found that for a range of concentrations between ~1×10^0 and 1×10^6 ppb of ash in snow, the albedo reduction was ~0–37% for clear-sky conditions. The largest deposit concentration in *Dadic et al*. [2013] was 2 orders of magnitude smaller than the largest deposit concentration reported here, either because *Dadic et al*. [2013] was only considering ash located a greater distance from the volcanic source, the eruptions which produced the ash were of a smaller scale, or more mixing of ash with snow had occurred. At an ash concentration of 2.8×10^7 ppb (~200 km from the vent), we calculate an albedo reduction of ~37% for new snow, which is similar to what *Dadic et al*. [2013] computed as the largest albedo reduction for the highest ash concentration. However, these studies are not directly comparable, because deposit concentrations from *Dadic et al*. [2013] included all ash sizes, while this study only focuses on aerosol-sized

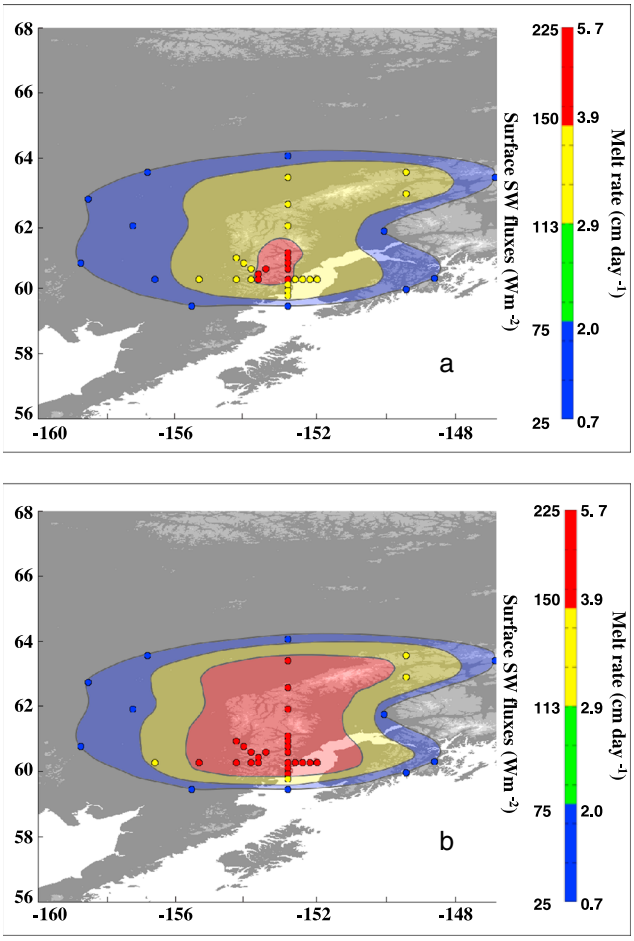

Figure 4. Range of realistic daily mean surface solar net clear-sky fluxes in W m^{-2} and estimated snow melt rates in cm d^{-1} calculated for $T_d = 0$°C from equation (1). (a) Ash deposits on new snow (effective radius = 100 μm) and (b) ash deposits on old snow (effective radius = 1000 μm). Note that Fall3D and SNICAR are not coupled, so fields were drawn based on calculations made at several points, which are denoted by circles.

ash deposits. Hence, the albedo changes for this study would be expected to be even more extreme if calculated in the same manner as *Dadic et al*. [2013], further demonstrating the capabilities of midsized eruptions to significantly alter surface albedo.

Shortwave surface net flux fields are defined as the difference between incoming and outgoing surface shortwave radiation (Figure 4). The shortwave surface net clear-sky fluxes for pure snow are 38.1 W m^{-2} for new snow and 65.2 W m^{-2} for aged snow. The net fluxes associated with ash deposits on snow ranged from 38.7 to 162 W m^{-2} for new snow and 65.9 to 222 W m^{-2} for aged snow. Since these values were all computed at a typical daily mean SZA, they approximate daily (12 h) averages for late March. As a comparison to similar work, *Skiles et al*. [2012] calculated springtime daily (24 h) mean forcings for dust deposits on snow in Colorado to be ~35–70 W m^{-2}, corresponding to concentrations of 2×10^5–4×10^6 ppb, respectively. The mean daily forcings due to dust deposits in the Arctic would be expected to be much less than those reported in Colorado because mean dust concentrations in the Arctic are reported to be ~2 and 3 orders of magnitude lower [i.e., *Zdanowicz et al*., 1998], and the incident solar radiation is reduced at higher latitudes. When forcings for ash deposition from this eruption are calculated using the method put forth in *Skiles et al*. [2012] and *Painter et al*. [2007], minimum forcing values due only to the direct effects of ash deposition onto snow range from ~0 to 96 W m^{-2}, from the outermost deposits to the vent.

A range of possible total snowmelt was estimated from shortwave surface net fluxes. It should be noted that modeled ash deposit thicknesses for these events totaled to < 1 cm. This is important because layers in excess of ~2.4 cm tend to insulate rather than melt the snow [*Driedger*, 1981]. According to equation (1), snowmelt occurs when the average daily surface temperature warms to above 0°C, which normally occurs at the end of March to early to mid-April, according to SNOTEL. Snowmelt may also occur even in subzero temperatures if the net solar flux is large enough. If snowmelt is calculated at 0°C, this will represent a lower bound on snowmelt amount and will quantify the melt that would be produced initially by radiative heating alone. This melting would cause further reduction in snow albedo, leading to increases in $F_{\mathrm{net,SW}}$ and surface temperature, which would cause more snowmelt. Figure 4 shows snowmelt fields for ash deposits over new and aged snow at 0°C. The snowmelt ranges for new snow are ~1.0–4.2 cm d^{-1} with the highest snowmelt near the vent and the lowest value at the edges of the deposits. According to *Driedger* [1981], if the ash layer thickness is larger than ~0.3 cm, heat conduction begins to slow and starts to offset radiative heating. Between ash thicknesses of 0.3–2.4 cm, the snow will melt but at a slower rate because the ash is starting to insulate it. Therefore, the melting rate reported here is an upper bound for regions very close to the volcanic vent, where thicknesses exceed ~0.3 cm. For old snow, the ranges are ~1.8–5.8 cm d^{-1}. Pure snow

at 0°C melts at a rate of ~1.0 cm d^{-1} for new snow and ~1.8 cm d^{-1} for old snow; therefore, no significantly accelerated snowmelts are expected on the edges of the deposits. However, for areas of higher ash loadings/concentrations, daily melt rates are significantly higher (~220–320%), but these regions include layers exceeding 0.3 cm. More conservative estimates of snowmelt rates may be calculated over regions of intermediate loadings (i.e., up to ~1.6×10^7 ppb for regions such as Skwentna), which yield maximum melt rates ~140–160% higher than those of pure snow. These estimates are in keeping with maximum snowmelt rates measured for artificially ash covered snow plots by *Driedger* [1981], which reports conservative maximum snowmelt increases of at least 90% over ash-free conditions. Many of the higher melt rates were found in mountainous areas where snow would be expected to melt later in the year. Early and accelerated snowmelts can be expected to lead to depletion of runoff in later months and shortages of water resources [*Qian et al.*, 2009].

4. Conclusions

The SNICAR model was used to calculate a range of realistic possible albedo change, forcing, and snowmelt that can be expected for ash deposits onto snow and ice from a typical midsized sub-Arctic eruption, using field and satellite constrained loading and ash grain sizes from the 2009 eruption of Redoubt volcano. The results presented here demonstrate the importance of volcanic ash deposits from midsized eruptions on surface albedo, surface radiative forcing, and snow melt rate. Because of the large estimated concentrations of ash in snow that ranged from ~6.9×10^4 to 1×10^8 ppb from the distal edge of the deposits (~100–570 km from the vent) to the vent, volcanic ash deposits had much larger radiative impacts over the region that was explored in this study when compared to other types of deposits typical to the Arctic, such as black carbon and dust.

We have shown that during midsize volcanic eruptions in the Arctic, near-vent ash loadings could be great enough to insulate the snow, but the majority of the deposit may be much thinner (<2.4 cm) and can therefore be a major agent of deposit-induced snowmelt. Although these calculations have been done for an eruption that was classified as midsized (based on the VEI), there have been notable larger eruptions in the Arctic and sub-Arctic's past (e.g., Laki, 1783 and Novarupta-Katmai, 1912). It may be that larger eruptions under weak wind conditions would tend to deposit enough ash to insulate the snow rather than melt it. However, larger eruptions under strong winds could disperse thinner layers of ash over larger areas, thereby having a larger radiative impact. Even small eruptions under weaker winds could cause sizeable albedo change and snowmelt, albeit over smaller areas. More studies are needed to determine the radiative impacts of different sizes of eruptions under varying meteorological conditions in the Arctic.

Future studies will include improving ash loading estimates and the acquisition of eruption-specific snow and ash properties for the SNICAR model [e.g., *Flanner et al.*, 2014]. Because of the lack of satellite data that is often problematic for this region due to the presence of clouds and the high-surface reflectivity, field measurements of albedo change and snow ablation rates would be very useful. These quantities are typically not measured because field excursions are difficult to plan due to the unpredictability and dangers of volcanic eruptions. Perhaps, the best field approach is to coordinate efforts with scientists at volcano observatories, supplying them with the instruments and methodologies to make these measurements. If field measurements are not possible, conditions could be simulated on a smaller scale in the lab. In addition, the radiative calculations done here could be made more sophisticated by coupling volcanic eruption source conditions, transport, and deposition, along with the SNICAR model, to a general circulation model, which would allow for the calculation of global effects. The vegetation fraction and the surface emissivity change caused by ash deposits on snow could also be considered in future snowmelt calculations. Clouds are often present in Arctic and sub-Arctic regions, and their effects on the radiative impacts in the presence of volcanic ash deposits should be investigated in the future.

Acknowledgments
The data presented in this paper are available in the supporting information and upon request from the corresponding author. The authors thank two anonymous reviewers whose comments improved this manuscript. Acknowledgment is given to Janet Schaefer and Kristi Wallace at AVO for providing snowfall data over ash deposits and stratigraphic information.

References

Clarke, A. D., and K. J. Noone (1985), Soot in the Arctic snowpack: A cause for perturbations in radiative transfer, *Atmos. Environ.*, *19*(12), 2045–2053, doi:10.1016/0004-6981(85)90113-1.

Conway, H., A. Gades, and C. F. Raymond (1996), Albedo of dirty snow during conditions of melt, *Water Resour. Res.*, *32*(6), 1713–1718, doi:10.1029/96WR00712.

Costa, A., G. Macedonio, and A. Folch (2006), A three-dimensional Eulerian model for transport and deposition of volcanic ashes, *Earth Planet. Sci. Lett.*, *241*(3–4), 634–647, doi:10.1016/j.epsl.2005.11.019.

Curry, J. A., W. B. Rossow, D. Randall, and J. L. Schramm (1996), Overview of Arctic cloud and radiation characteristics, *J. Clim.*, *9*(8), 1731–1764, doi:10.1175/1520-0442(1996)009<1731:OOACAR>2.0.CO;2.
Dadic, R., P. C. Mullen, M. Schneebeli, R. E. Brandt, and S. G. Warren (2013), Effects of bubbles, cracks, and volcanic tephra on the spectral albedo of bare ice near the Transantarctic Mountains: Implications for sea glaciers on snowball Earth, *J. Geophys. Res. Earth Surf.*, *118*, 1658–1676, doi:10.1002/jgrf.20098.
Driedger, C. (1981), Effect of ash thickness on snow ablation, in *The 1980 Eruptions of Mount St. Helens, Washington*, edited by P. W. Lipman and R. L. Christiansen, *U.S. Geol. Surv. Prof. Pap., 1250*, 757–760.
Flanner, M. G., and C. S. Zender (2005), Snowpack radiative heating: Influence on Tibetan Plateau climate, *Geophys. Res. Lett.*, *32*, L06501, doi:10.1029/2004GL022076.
Flanner, M. G., and C. S. Zender (2006), Linking snowpack microphysics and albedo evolution, *J. Geophys. Res.*, *111*, D12208, doi:10.1029/2005JD006834.
Flanner, M. G., C. S. Zender, J. T. Randerson, and P. J. Rasch (2007), Present-day climate forcing and response from black carbon in snow, *J. Geophys. Res.*, *112*, D11202, doi:10.1029/2006JD008003.
Flanner, M. G., A. S. Gardner, S. Eckhardt, A. Stohl, and J. Perket (2014), Aerosol radiative forcing from the 2010 Eyjafjallajökull volcanic eruptions, *J. Geophys. Res. Atmos.*, *119*, 9481–9491, doi:10.1002/2014JD021977.
Folch, A., A. Costa, and G. Macedonio (2009), FALL3D: A computational model for transport and deposition of volcanic ash, *Comput. Geosci.*, *35*(6), 1334–1342, doi:10.1016/j.cageo.2008.08.008.
Fu, Q., T. J. Thorsen, J. Su, J. M. Ge, and J. P. Huang (2009), Test of Mie-based single-scattering properties of non-spherical dust aerosols in radiative flux calculations, *J. Quant. Spectros. Radiat. Transfer*, *110*(14), 1640–1653, doi:10.1016/j.jqsrt.2009.03.010.
Knap, W. H., C. H. Reijmer, and J. Oerlemans (1999), Narrowband to broadband conversion of Landsat TM glacier albedos, *Int. J. Remote Sens.*, *20*(10), 2091–2110.
Kustas, W. P., A. Rango, and R. Uijlenhoet (1994), A simple energy budget algorithm for the snowmelt runoff model, *Water Resour. Res.*, *30*(5), 1515–1527, doi:10.1029/94WR00152.
Langen, P. L., and V. A. Alexeev (2007), Polar amplification as a preferred response in an idealized aquaplanet GCM, *Clim. Dyn.*, *29*(2–3), 305–317, doi:10.1007/s00382-006-0221-x.
Martinec, J. (1989), Hour-to-hour snowmelt rates and lysimeter outflow during an entire ablation period, in *Proceedings of the Baltimore Symposium: Snow Cover and Glacier Variations, Baltimore, Maryland*, *Publ. 183*, pp. 19–28, IAHS, Wallingford, U. K.
Mastin, L. G., H. Schwaiger, D. J. Schneider, K. L. Wallace, J. Schaefer, and R. P. Denlinger (2013), Injection, transport, and deposition of tephra during event 5 at Redoubt volcano, 23 March, 2009, *J. Volcanol. Geotherm. Res.*, *259*, 201–213, doi:10.1016/j.jvolgeores.2012.04.025.
McConnell, J. R., R. Edwards, G. L. Kok, M. G. Flanner, C. S. Zender, E. S. Saltzman, J. R. Banta, D. R. Pasteris, M. M. Carter, and J. D. W. Kahl (2007), 20th-century industrial black carbon emissions altered arctic climate forcing, *Science*, *317*(5843), 1381–1384, doi:10.1126/science.1144856.
Melloh, R. A. (1999), *A Synopsis and Comparison of Selected Snowmelt Algorithms*, *CRREL-99-8*, Cold Reg. Res. and Eng. Lab., Hanover, N. H.
Painter, T. H., J. Dozier, D. A. Roberts, R. E. Davis, and R. O. Green (2003), Retrieval of subpixel snow-covered area and grain size from imaging spectrometer data, *Remote Sens. Environ.*, *85*(1), 64–77, doi:10.1016/S0034-4257(02)00187-6.
Painter, T. H., A. P. Barrett, C. C. Landry, J. C. Neff, M. P. Cassidy, C. R. Lawrence, K. E. McBride, and G. L. Farmer (2007), Impact of disturbed desert soils on duration of mountain snow cover, *Geophys. Res. Lett.*, *34*, L12502, doi:10.1029/2007GL030284.
Painter, T. H., J. S. Deems, J. Belnap, A. F. Hamlet, C. C. Landry, and B. Udall (2010), Response of Colorado River runoff to dust radiative forcing in snow, *Proc. Natl. Acad. Sci. U.S.A.*, *107*(40), 17,125–17,130, doi:10.1073/pnas.0913139107.
Pollack, J. B., O. B. Toon, and B. N. Khare (1973), Optical properties of terrestrial rocks and glasses, *Icarus*, *19*, 372–389, doi:10.1016/0019-1035(73)90115-2.
Qian, Y., W. I. Gustafson, L. R. Leung, and S. J. Ghan (2009), Effects of soot-induced snow albedo change on snowpack and hydrological cycle in western United States based on Weather Research and Forecasting chemistry and regional climate simulations, *J. Geophys. Res.*, *114*, D03108, doi:10.1029/2008JD011039.
Quinn, P. K., et al. (2008), Short-lived pollutants in the Arctic: Their climate impact and possible mitigation strategies, *Atmos. Chem. Phys.*, *8*, 1723–1735, doi:10.5194/acp-8-1723-2008.
Schaefer, J. R. (2012), *The 2009 Eruption of Redoubt Volcano, Alaska*, *Report of Investigations RI 2011-5*, contributed by K. P. Bull et al., State of Alaska, Dep. of Nat. Resour., Div. of Geol. and Geophys. Surv., Fairbanks, Alaska.
Schaefer, J. R., and K. L. Wallace (2012), *Ash Fall Contour Map of the 2009 Eruption of Redoubt Volcano, Alaska: Digital Shapefiles of Contours and Sample Locations*, *Miscellaneous Publication MP 143*, State of Alaska, Dep. of Nat. Resour., Div. of Geol. and Geophys. Surv., Fairbanks, Alaska.
Shindell, D. (2007), Local and remote contributions to Arctic warming, *Geophys. Res. Lett.*, *34*, L14704, doi:10.1029/2007GL030221.
Simkin, T., and L. Siebert (1994), *Volcanoes of the World*, 2nd ed., 368 pp., Geoscience Press, Tucson, Ariz.
Skiles, S. M., T. H. Painter, J. S. Deems, A. C. Bryant, and C. C. Landry (2012), Dust radiative forcing in snow of the Upper Colorado River Basin: 2. Interannual variability in radiative forcing and snowmelt rates, *Water Resour. Res.*, *48*, W07522, doi:10.1029/2012WR011986.
Smith, A. J. A., and R. G. Grainger (2014), Does variation in mineral composition alter the short-wave light scattering properties of desert dust aerosol?, *J. Quant. Spectrosc. Radiat. Transfer*, *133*, 235–243, doi:10.1016/j.jqsrt.2013.08.005.
Stone, R. S., G. P. Anderson, E. Andrews, E. G. Dutton, E. P. Shettle, and A. Berk (2007), Incursions and radiative impact of Asian dust in northern Alaska, *Geophys. Res. Lett.*, *34*, L14815, doi:10.1029/2007GL029878.
Stone, R. S., G. P. Anderson, E. P. Shettle, E. Andrews, K. Loukachine, E. G. Dutton, C. Schaaf, and M. O. Roman (2008), Radiative impact of boreal smoke in the Arctic: Observed and modeled, *J. Geophys. Res.*, *113*, D14S16, doi:10.1029/2007JD009657.
Toon, O. B., C. P. McKay, T. P. Ackerman, and K. Santhanam (1989), Rapid calculation of radiative heating rates and photodissociation rates in inhomogeneous multiple scattering atmospheres, *J. Geophys. Res.*, *94*(D13), 16,287–16,301, doi:10.1029/JD094iD13p16287.
Tsvetsinskaya, E. A., C. B. Schaaf, F. Gao, A. H. Strahler, R. E. Dickinson, X. Zeng, and W. Lucht (2002), Relating MODIS-derived surface albedo to soils and rock types over Northern Africa and the Arabian peninsula, *Geophys. Res. Lett.*, *29*(9), 1353, doi:10.1029/2001GL014096.
Wallace, K. L., J. R. Schaefer, and M. L. Coombs (2013), Character, mass, distribution, and origin of tephra-fall deposits from the 2009 eruption of Redoubt volcano, Alaska—Highlighting the significance of particle aggregation, *J. Volcanol. Geotherm. Res.*, *259*, 145–169, doi:10.1016/j.jvolgeores.2012.09.015.
Wang, L., Z. Li, Q. Tian, Y. Ma, F. Zhang, Y. Zhang, D. Li, K. Li, and L. Li (2013), Estimate of aerosol absorbing components of black carbon, brown carbon, and dust from ground-based remote sensing data of Sun-sky radiometers, *J. Geophys. Res. Atmos.*, *118*, 6534–6543, doi:10.1002/jgrd.50356.
Warren, S. G. (1984), Impurities in snow: Effects on albedo and snowmelt, *Ann. Glaciol.*, *5*, 177–179.
Warren, S. G., and W. J. Wiscombe (1985), Dirty snow after nuclear war, *Nature*, *313*(6002), 467–470.

Warren, S. G., R. E. Brandt, and T. C. Grenfell (2006), Visible and near-ultraviolet absorption spectrum of ice from transmission of solar radiation into snow, *Appl. Opt.*, *45*(21), 5320–5334, doi:10.1364/AO.45.005320.

Young, C. L., I. N. Sokolik, and J. Dufek (2012), Regional radiative impact of volcanic aerosol from the 2009 eruption of Mt. Redoubt, *Atmos. Chem. Phys.*, *12*(8), 3699–3715, doi:10.5194/acp-12-3699-2012.

Young, C. L., J. Dufek, and I. N. Sokolik (2014), Assessment of depositional ash loading from the 2009 eruption of Mt. Redoubt, *J. Volcanol. Geotherm. Res.*, *274*, 122–138, doi:10.1016/j.jvolgeores.2014.02.003.

Zdanowicz, C. M., A. Zielinksi, and C. P. Wake (1998), Characteristics of modern atmospheric dust deposition in snow on the Penny Ice Cap, Baffin Island, Arctic Canada, *Tellus Ser. B*, *50*, 506–520, doi:10.1034/j.1600-0889.1998.t01-1-00008.x.